Check for updates

Designing amphiphilic Janus nanoparticles with tunable lipid raft affinity *via* molecular dynamics simulation†

Xiaoqian Lin [ID] [a,b] and Xubo Lin [ID] *[a]

Due to the differential interactions among lipids and proteins, the plasma membrane can segregate into a series of functional nanoscale membrane domains ("lipid rafts"), which are essential in multiple biological processes such as signaling transduction, protein trafficking and endocytosis. On the other hand, Janus nanoparticles (NPs) have shown great promise in various biomedical applications due to their asymmetric characteristics and can integrate different surface properties and thus synergetic functions. Hence, in this work, we aim to design an amphiphilic Janus NP to target and regulate lipid rafts *via* tuning its surface ligand amphiphilicity using coarse-grained molecular dynamics (MD) simulations. Our µs-scale free coarse-grained MD simulations as well as umbrella sampling free energy calculations indicated that the hydrophobicity of the hydrophobic surface ligands not only determined the lateral membrane partitioning thermodynamics of Janus NPs in phase-separated lipid membranes, but also the difficulty in their insertion into different membrane domains of the lipid membrane. These two factors jointly regulated the lipid raft affinity of Janus NPs. Meanwhile, the hydrophilicity of the hydrophilic surface ligands could affect the insertion ability of Janus NPs. Besides, the ultra-small size could ensure the membrane-bound behavior of Janus NPs without disrupting the overall structure and phase separation kinetics of the lipid membrane. These results may provide valuable insights into the design of functional NPs targeting and controllably regulating lipid rafts.

Introduction

The plasma membrane can segregate into a series of membrane domains with different properties due to the differential interactions among different lipids and proteins. Among them, nanoscale dynamic functional membrane domains are defined as "lipid rafts".[1–3] Generally, the dynamics of lipid rafts can be divided into *intra-leaflet* and *inter-leaflet* parts. The *intra-leaflet* dynamics is mainly dominated by the difference between lipid raft and non-raft domains,[4,5] which can be also affected by embedded nanoparticles (NPs)/molecules.[6,7] The *inter-leaflet* dynamics is determined by the *inter-leaflet* coupling strength, which is jointly modulated by several factors including lipid chain inter-digitation,[8] cholesterol flip-flop rate[9] and lipid chain *cis* double bond position.[10] The lipid raft

dynamics is tightly correlated to its essential roles in various biological processes such as endocytosis,[11,12] membrane trafficking[13,14] and immune signaling.[15] The destruction of these processes will induce many diseases.[16] Hence, lipid rafts can serve as important targets for regulating these processes.

Due to the unique properties brought by the small size effect, NPs have been widely used for various biomedical applications such as bio-imaging,[17] bio-sensing,[18] drug delivery[19] and theranostics.[20] Atomic-scale interactions between NPs with different physicochemical properties and the cell membrane revealed by molecular dynamics (MD) simulations[21–23] and cell/molecular biology experiments[24,25] can help reduce the possible toxicity for safer and more effective biomedical applications of NPs. On the other hand, the development of NPs integrating more features may help promote NPs' application potential. Amphiphilic Janus NPs,[26–28] which have half hydrophilic ligands and half hydrophobic ligands, belong to this category. In particular, the usage of Janus NPs for targeting and regulating the cell membrane has attracted much attention in the past decade.[6,29–32] Lee *et al.*[6,29,30] studied the interactions between supported lipid bilayers and amphiphilic Janus NPs with different ratios of hydrophilic and hydrophobic surface ligands using *in vitro* experiments and dissipative par-

[a]Institute of Single Cell Engineering, Key Laboratory of Ministry of Education for Biomechanics and Mechanobiology, Beijing Advanced Innovation Center for Biomedical Engineering, School of Biological Science and Medical Engineering, Beihang University, Beijing 100191, China. E-mail: linxbseu@buaa.edu.cn
[b]Shen Yuan Honors College, Beihang University, Beijing 100191, China
†Electronic supplementary information (ESI) available: Additional supplementary analysis and figures. See DOI: 10.1039/d1bm01364e

ticle dynamics simulations. They found that Janus NPs over a certain concentration could induce membrane poration. Using atomistic MD simulations, Liang and coauthors investigated the interactions between amphiphilic Janus NPs and symmetric/asymmetric lipid bilayers.[31] The result indicated that Janus NPs could easily insert into the liquid-disordered and asymmetric lipid bilayers, which might be jointly affected by several factors including the surface ligand's hydrophobicity, the lipid order and the bilayer's curvature. In other words, it will be possible to design a Janus NP with tunable raft affinity by changing the physicochemical properties of its surface ligands, which may target lipid rafts and regulate the corresponding biological processes.

Coarse-grained models, which map several heavy atoms into one interaction site, allow much longer time and space scales of MD simulations and thus provide useful tools to directly study the phase-separated lipid membranes (model lipid raft systems).[10,33] Hence, in this work, we aim to design Janus NPs with different physicochemical properties of surface ligands for tunable raft affinity using coarse-grained MD simulations. Spherical NPs with high density of ligand loading are believed to obtain their unique properties through multivalent effects, which can lead to high-efficiency affinity for cell surface receptors.[34] Inspired from our previous studies,[22,23] we mainly focused on the hydrophobicity/hydrophilicity of surface ligands of 100%-modified Janus NPs. μs-Scale unbiased MD simulations were used to quantify the lateral membrane partitioning thermodynamics of Janus NPs in phase-separated lipid membranes. We further employed umbrella sampling simulations and the weighted histogram analysis method (WHAM) to calculate membrane insertion free energies for different Janus NPs into model lipid raft/non-raft membranes. The results provide helpful insights into the design of Janus NPs with tunable raft affinity.

Methods

Force field and system setup

For all our MD simulations in this work, we adopted the MARTINI coarse-grained force field[35] (version 2.0), which has been widely used for studying lipid membranes[36] and nanoparticles.[37] In the MARTINI force field, generally four heavy atoms are mapped into one interaction site ("coarse-grained bead"), except for ring structures, which use 2 or 3 to 1 mapping rule. Four main types of interaction sites (polar, P; nonpolar, N; apolar, C; charged, Q) are introduced. Each type has several subtypes to better capture the degree of polarity and hydrogen-bonding capabilities of the atomic structures. Details of the interaction matrix between different types can be found in the original paper.[35]

The amphiphilic Janus NPs were constructed using the following two steps. First, Martini coarse-grained beads (C5-type, suitable for gold NP[38]) were uniformly distributed on concentric spherical surfaces with the lattice constant of 0.47 nm to obtain the rigid NP core, which consisted of 59 coarse-

grained beads and had a diameter of 2.35 nm. Then, the smooth surface of the NP core was fully modified with 23 hydrophobic ligands on one half and 23 hydrophilic ligands on the other half, and each ligand consisted of 5 coarse-grained beads (Fig. 1a). Two hydrophobicity (C1: more hydrophobic; C5: less hydrophobic) and two hydrophilicity (P1: less hydrophilic; P5: more hydrophilic) were considered. Hence, four kinds of Janus NPs were studied in total, which were named C1–P1, C1–P5, C5–P1 and C5–P5 for clarity. PEG,[39,40] a hydrophilic protein[41] and a hydrophilic peptide[42] (PYY3-36) and other completely hydrophilic ligands in the experimental system can be modified on the NPs to play a certain biological role. Inspire by these related studies, we adopt the completely hydrophilic ligand on the half of Janus NPs.

The tool *insane.py*[43] was used to set up all membrane systems. Three-component lipid bilayers of dipalmitoyl-phosphatidylcholine (DPPC), dilinoleoyl-phosphatidylcholine (DUPC) and cholesterol (CHOL) in a molar ratio of $5:3:2$,[5] which consisted of 624 DPPC, 374 DUPC, 250 CHOL, 87 377 water molecules and 0.15 M NaCl (the initial box size is 20 nm × 20 nm × 30 nm), were used to model phase-separated membranes. Besides, we employed a two-component lipid bilayer of DPPC and CHOL ($5:2$) and a pure DUPC bilayer for L_o and L_d membrane domains. The former membrane system contained 458 DPPC, 182 CHOL, 31 294 water molecules and 0.15 M NaCl (the initial box size is 15 nm × 15 nm × 20 nm). The latter was made up of 642 DUPC, 31 292 water molecules and 0.15 M NaCl (the initial box size is 15 nm × 15 nm × 20 nm). The Martini-based configurations of DPPC, DUPC, and CHOL are illustrated in Fig. 1b. Among them, a DPPC/DUPC molecule is comprised of 12 CG beads. A CHOL molecule is comprised of 8 CG beads.
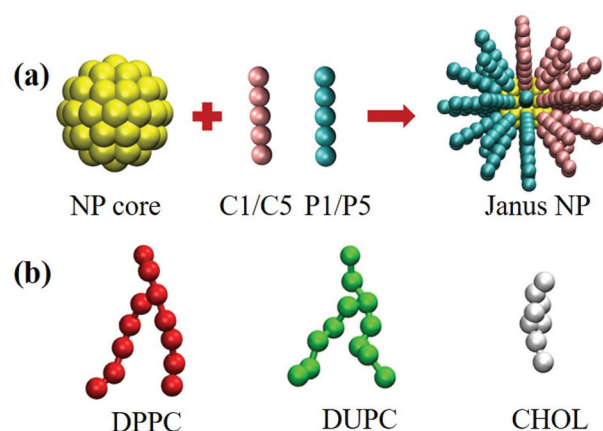

Fig. 1 Schematic illustration of the Janus NPs and coarse-grained lipids used in this work. (a) Ligand-modified Janus NPs with different ligand properties. The NP core (C5) is colored in yellow, hydrophobic ligand (C1/C5) in pink, hydrophilic ligand (P1/P5) in cyan. (b) Saturated lipids (DPPC), unsaturated lipids (DUPC) and cholesterol (CHOL). DPPC is colored in red, DUPC in green, CHOL in white. Snapshots in this work are generated by VMD.[47]

Molecular dynamics simulation

In this work, all coarse-grained MD simulations were run using GROMACS (version 5.1.5)[44] under constant particle, pressure and temperature (NPT ensemble) as well as periodic boundary conditions. The semiisotropic Parrinello-Rahman pressure coupling scheme[45] is used to control the pressure at 1 bar in both the in-plane (x–y) and the normal (z) directions of the bilayer with a coupling constant $\tau = 5$ ps and compressibility of 3×10^{-4} bar^{-1}. The temperature was maintained at $T = 310$ K using v-rescale heat baths[46] with $\tau = 1$ ps. The Lennard-Jones potential, which was smoothly shifted to zero between 0.9 and 1.2 nm, was used to calculate van der Waals (vdW) interactions. Electrostatic interactions were calculated using the particle-mesh Ewald method with a real-space cutoff of 1.2 nm. The relative dielectric constant was 15, which is the default value of the force field.[35] For studying NP's membrane partitioning thermodynamics, the Janus NP was initially placed in the water region 4 nm above the three-component lipid bilayer. First, each system with a fixed NP was simulated at $T = 400$ K and the NPT ensemble for 10 ns to achieve the uniform lipid distribution. Second, the system was gradually adjusted to the body temperature ($T = 310$ K) and run for 2 μs to achieve full phase-separation of the lipid membrane. Third, the constraint of Janus NP was removed and dragged towards the lipid membrane until the hydrophobic ligands were fully inserted into the lipid membrane. Finally, each system was run for 4 μs with a time step of 20 fs and a trajectory-saving frequency of 500 ps. For each simulation system, at least two independent copies were performed. Besides, in order to validate that the initial insertion position of Janus NP does not affect its final membrane partitioning during our μs-scale simulation, the Janus NP was inserted into the opposite membrane position and the new system was run for several μs (Fig. S11†).

Umbrella sampling simulations

In order to quantify the difficulty of inserting different Janus NPs into the lipid membrane, we performed a series of umbrella sampling simulations to calculate the potential of mean force (PMF). The center-of-mass (COM) distance between the Janus NP and the L_o/L_d lipid membrane along the z axis was chosen as the reaction coordinate (ξ). 26 sampling simulations with ξ ranging from 0 to 5 nm ($\Delta\xi = 0.2$ nm) were performed. The zero points of the PMFs were set at the position ($\xi = 5$ nm) where NPs do not contact the lipid bilayer. In each simulation, ξ was constrained by the harmonic potentials with a force constant of 1500 kJ mol^{-1} nm^{-2} and each umbrella window was run for 500 ns. PMF profiles were calculated using the weighted histogram analysis method[48] over the last 400 ns of each 500 ns trajectory (Fig. S10†). To determine the convergence of PMF calculations, standard deviations from the block averaging with four 100 ns blocks were used.

Analysis of trajectories

Two-dimensional (2D) number-density map. In order to explore the localization of amphiphilic Janus NPs in the lipid membrane, the combination of the 2D number density map of DPPC molecules and the motion tracking of Janus NPs was used. The former was generated by the GROMACS tool *gmx densmap*[44] over the last 500 ns trajectory, where the high probability region (red), the intermediate probability region (green) and low probability region (blue) correspond to L_o, the interface and L_d domains. The latter was achieved *via* the GROMACS tool *gmx traj*[44] for the COM coordinates of the Janus NP over the same period. These discrete points were plotted in the same 2D (x–y) plane. By overlapping the data of the two analyses, the relative partition preferences of Janus NPs can be determined.

Contact ratio of Janus NP with the L_o/L_d membrane domain. GROMACS tool *gmx mindist* (cutoff: 0.6 nm) was used to calculate the contact number of the Janus NP with L_o domain lipids (DPPC & CHOL) and L_d domain lipids (DUPC), which can be used to calculate the contact ratio of the JNP with the L_o/L_d membrane domain and help reveal the effects of NP's surface physicochemical properties on their preferred membrane localization.

Lipid chain order parameter. Lipid chain order parameter (S_z) can be calculated with the formula

$$S_{z,n} = \left\langle \frac{1}{2} \left(3 \cos^2 \theta_n - 1 \right) \right\rangle$$

where θ_n is the angle between the vector connecting the $n - 1$ and $n + 1$ beads of the lipid tail and the membrane normal z, and the lipid chain order parameter is the average over the two chains of the same lipids in the entire bilayer to compare lipid chain order parameters among different systems.

Voronoi tessellation analysis. To quantify the disruption to the local packing of the lipid membrane by the Janus NP, we performed Voronoi tessellation analysis in MATLAB over the x–y components of DPPC/DUPC COM coordinates. CHOL was not considered due to its flip-flop properties. In this analysis, the lipid bilayer plane was separated into polygonal regions based on the vertical bisector of two adjacent points. Each polygonal region represents the area of a single lipid. For visualization, the area per lipid was directly colored with the area value. The detailed procedures as well as the corresponding commands for MATLAB are provided in the ESI.†

Membrane thickness. In order to quantify the local effects of the Janus NP on the membrane thickness, the 2D membrane thickness map was visualized. In this analysis, 16 × 16 mesh grids were applied to the upper and lower membrane leaflets separately. Within each grid, the membrane thickness was calculated by the differences between the maximum z-coordinate of upper lipids and the minimum z-coordinate of lower lipids, which is further averaged over the selected period of MD trajectory. After obtaining the average membrane thickness for each grid, the 2D membrane thickness map was reconstructed by MATLAB. Additionally, periodic boundary conditions and interpolation fitting were performed to reduce edge effects between the neighboring mesh grids.

View Article Online

Paper

Biomaterials Science

Results and discussion

Ligand hydrophobicity of the amphiphilic Janus NP determines the lateral partitioning thermodynamics in phase-separated lipid membranes

In this work, we focused on four amphiphilic Janus NPs with two ligand hydrophobicity (C1, C5) and two ligand hydrophilicity (P1, P5) as mentioned in the Methods section. First, a coarse-grained MD simulation of the DPPC/DUPC/CHOL lipid bilayer with all molecules evenly distributed was run as long as 2 μs, which could make sure the fully phase separation of the membrane.[7,49–51] The rotational motion of Janus NPs, which were placed in the water region 4 nm above the phase-separated lipid membrane, may induce their hydrophilic ligands close to lipid membrane, such that it will take a long time for them to be spontaneously inserted into the lipid membrane.[52] However, the focus of our unbiased MD simulations is to reveal the lateral membrane partitioning preferences of the inserted Janus NPs. In view of this, a force was imposed on each NP to drag it towards the lipid membrane and their hydrophobic ligands quickly inserted themselves into the lipid membrane. Then, the force was removed and the obtained system conformation was used for the subsequent unbiased MD simulation. Finally, 4 μs coarse-grained MD simulations were performed for each Janus NP.

In all cases, Janus NPs kept the membrane-bound state stable over the whole simulation time. As shown in the simulation snapshots (Fig. 2a), Janus NPs with more hydrophobic (C1) ligands tend to locate in the L_o membrane domain (red region), while less hydrophobic (C5) ligands can drag Janus NPs fully into the L_d membrane domain (green region). The role of the ligand hydrophobicity of membrane-bound Janus NPs in the lateral membrane partitioning thermodynamics reported here is consistent with the previous work of fully hydrophobic NPs,[22,23] which are embedded inside the lipid membrane. In order to further confirm the lateral membrane partitioning thermodynamics of these Janus NPs, we first obtained the 2D number density map of the DPPC molecules and tracked the position of Janus NPs over the last 500 ns of each trajectory (Fig. 2b). Then, the contact ratios of Janus NPs with L_o (DPPC and CHOL) and L_d (DUPC) domain lipids over the whole simulation time (Fig. 2c and Fig. S1–2†) were calculated. Consistent with simulation snapshots (Fig. 1a), these results quantitatively indicate that Janus NPs with more hydrophobic (C1) ligands prefer the L_o membrane domain much more than Janus NPs with less hydrophobic (C5) ligands. Moreover, when the hydrophilic ligands change from less hydrophilic (P1) to more hydrophilic (P5), Janus NP's preference to the L_o membrane domain is further enhanced, which is very obvious for the more hydrophobic (C1) ligands. In other words, the raft affinity of these Janus NPs agrees with the following order: C1–P5 > C1–P1 > C5–P1 or C5–P5. The raft affinity of the amphiphilic Janus NP is mainly determined by its ligand hydrophobicity, which can also be affected by the ligand hydrophilicity.

For the role of the ligand hydrophobicity, it can be explained by different interactions between different coarse-
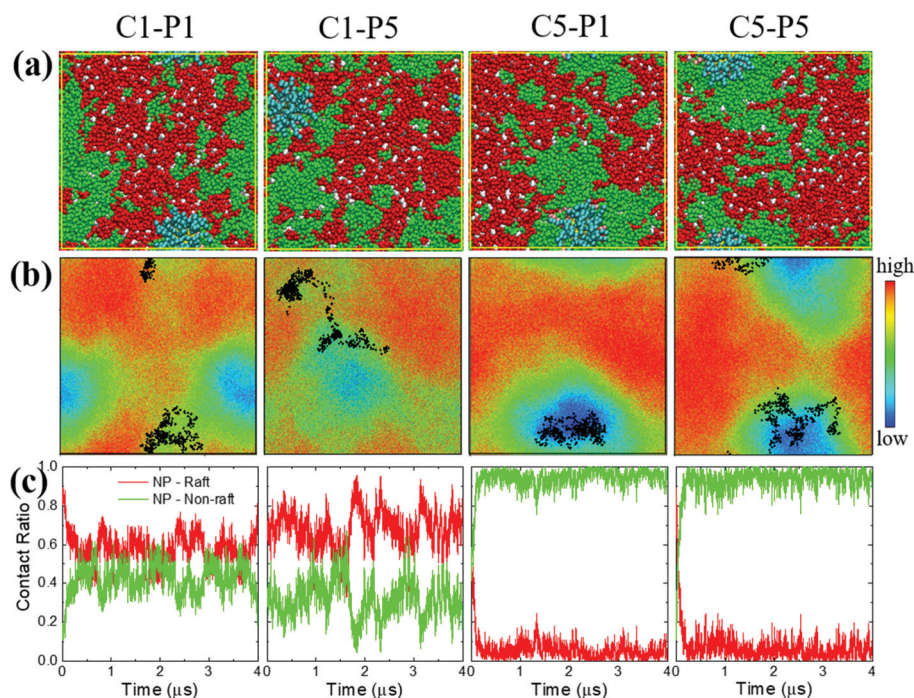

Fig. 2 Effects of ligand properties on the lateral membrane partitioning dynamics of ligand-modified Janus NPs. (a) Top-view system snapshots of the last frame of each 4 μs trajectory. The coloring style is the same as in Fig. 1. (b) 2D number-density maps of DPPC molecules and the instantaneous location of Janus NP (black points) derived from analysis over the last 500 ns trajectory. (c) Time evolution of the contact ratio of Janus NPs with raft/non-raft domains.

8252 | Biomater. Sci., 2021, **9**, 8249–8258

This journal is © The Royal Society of Chemistry 2021

grained beads (Table S1†). In the MARTINI coarse-grained model,[35] the two tails of the DPPC molecule are composed of solely C1 beads, while DUPC tails contain both C1 and C4 beads. Among coarse-grained C1, C4 and C5 beads, C1 prefers to interact with C1 rather than C4. In contrast, C5 is more attractive to C4 than C1. It is this interaction difference that drives the preferences of more hydrophobic (C1) and less hydrophobic (C5) ligands to DPPC-rich (L_o) and DUPC-rich (L_d) membrane domains correspondingly. However, as for the role of the ligand hydrophilicity, direct interaction differences between hydrophilic ligands and lipids may not be able to explain it because the presence of hydrophobic ligands prevents their direct interactions (Fig. 3a). Hence, we turn to the interactions between hydrophilic ligands and water molecules. Compared to less hydrophilic (P1) ligands, more hydrophilic (P5) ligands prefer to interact with water (P4) molecules (Table S1†). This difference will induce different membrane insertion depths of amphiphilic Janus NPs. As shown in Fig. 3b, the COM distance between the Janus NP and the lipid membrane clearly indicated that stronger interactions between more hydrophilic (P5) ligands and water molecules can pull out Janus NPs from the lipid membrane to a certain degree. In other words, C1–P5 and C5–P5 have less membrane insertion

depths than C1–P1 and C5–P1 respectively. The differences in the membrane insertion depth will inevitably change the lateral diffusion ability of Janus NPs (Fig. 2b), which thus may affect NP's lipid raft affinity.

Ligand amphiphilicity affects the targeting of Janus NP to the lipid membrane

As discussed above, the lateral membrane partitioning thermodynamics of membrane-bound amphiphilic Janus NPs can be mainly regulated by their hydrophobic ligands and partly affected by their hydrophilic ligands. In other words, the ligand amphiphilicity determined the raft affinity of Janus NPs after they inserted themselves into the lipid membrane. However, it is still not clear whether the ligand amphiphilicity can affect the targeting to lipid raft or non-raft membranes from the bulk water region. In order to clarify this, we performed umbrella sampling simulations and WHAM analysis for the membrane insertion free energy profiles of these Janus NPs. As shown in Fig. 4, there is an obvious energy minimum for each PMF profile, which corresponds to the optimal membrane insertion depth (ξ) of the Janus NP. The existence of these minima can be ascribed to the presence of hydrophobic and hydrophilic ligands. The former have preferred attractive
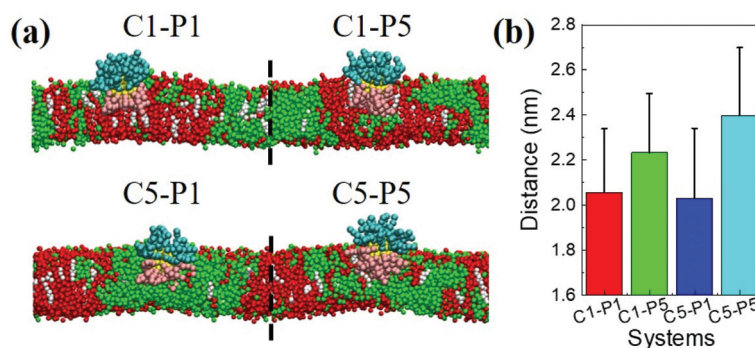

Fig. 3 Effects of ligand hydrophilicity on the embedding depth of the ligand-modified Janus NPs into the membrane. (a) Side-view system snapshots of the last frame of each 4 μs trajectory. The coloring style is the same as in Fig. 1. (b) COM distance between Janus NPs and the lipid bilayers derived from analysis over the last 2 μs trajectory.
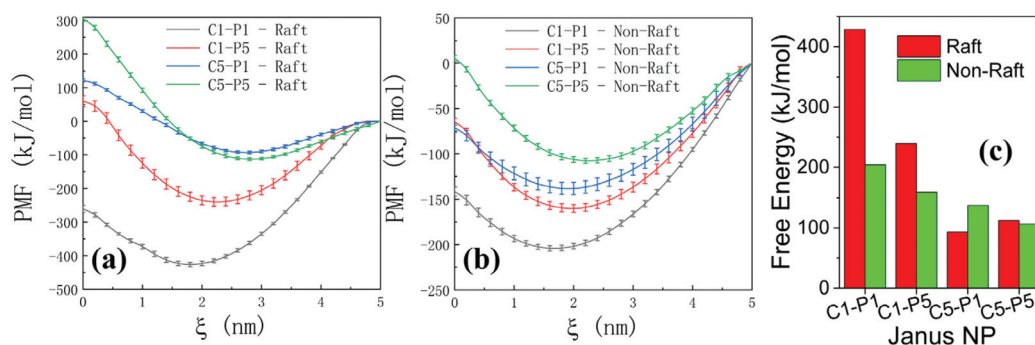

Fig. 4 The PMF profiles for Janus NPs translocating into lipid raft (a) and non-raft (b) membrane domains. Error bars are standard deviations based on statistics from four 100 ns blocks over last 400 ns of the trajectory and are drawn as lines with caps. (c) Membrane insertion free energy of the Janus NP into raft-like and non-raft-like lipid membrane derived from (a) and (b).

interactions with lipid tails,[22,23] while the latter prefer water molecules and lipid head-groups.[50] These optimal depths for Janus NP insertion into raft-like/non-raft-like lipid membranes are more or less consistent with our previous results (Fig. 3b). When the Janus NP was further dragged into the membrane interior, a significant energy barrier appeared, which indicated that the amphiphilic Janus NP will prefer the membrane-bound state rather than the fully encapsulation into the hydrophobic region of the lipid bilayer. Hence, we can define an energy difference between the bulk water region (ξ = 5 nm) and the optimal insertion depth to quantify the membrane insertion difficulty of the Janus NP, which determines NP's targeting ability to either lipid raft or non-raft membrane domains.

Fig. 4c shows the membrane insertion free energy of each Janus NP into raft-like or non-raft-like lipid membranes. The results indicate that C1–P1 has the largest membrane insertion free energy for both raft-like and non-raft-like lipid membranes, which means that C1–P1 can easily insert into both raft-like and non-raft-like lipid membranes. Considering the large difference between these two insertion free energies, C1–P1 will preferably target the lipid raft from the bulk water region. Similarly, C1–P5 can also target the lipid raft from the bulk water region. However, compared to C1–P1, its targeting ability is greatly reduced due to the decreased membrane insertion free energy differences. For C5–P1, the membrane insertion free energy into the non-raft-like lipid membrane is much larger than that into the raft-like lipid membrane. In other words, C5–P1 can be used to target the lipid non-raft.

C5–P5 shows a similar preference to either raft-like or non-raft-like lipid membrane, and thus cannot be used to specifically target either lipid raft or non-raft. The differences in the targeting ability to the lipid raft induced by the different ligand hydrophobicity are consistent with the role of the lipid anchor type in determining the membrane localization of Ras proteins.[53,54] For the tested amphiphilic Janus NPs, more hydrophobic (C1) ligands ensure their targeting ability to the lipid raft, while less hydrophobic (C5) ligands prefer the lipid non-raft. When changing hydrophilic ligands to P5-type (more hydrophilic), both the raft targeting ability of the C1-Janus NP and the non-raft targeting ability of the C5-Janus NP are significantly weakened. In short, the targeting ability of Janus NPs to either lipid raft or non-raft is jointly modulated by the ligand amphiphilicity.

For the Janus NP in the water region, its raft affinity is reflected in two processes: (1) membrane insertion process, (2) lateral membrane partitioning process. Our PMF calculations (Fig. 4) clearly showed that all the tested amphiphilic Janus NPs could easily insert themselves into the lipid membrane and maintain the membrane-bound states. The differences in the insertion difficulty into raft/non-raft membrane domains contribute to the targeting preference from the water region to raft/non-raft membrane domains. The insertion difficulty of the Janus NP was jointly determined by the ligand amphiphilicity. When the Janus NP is inserted into the lipid membrane, its subsequent lateral membrane partitioning process is also jointly modulated by mainly the ligand hydrophobicity (Fig. 2) as well as the membrane domain stability.[50,55] In short, the
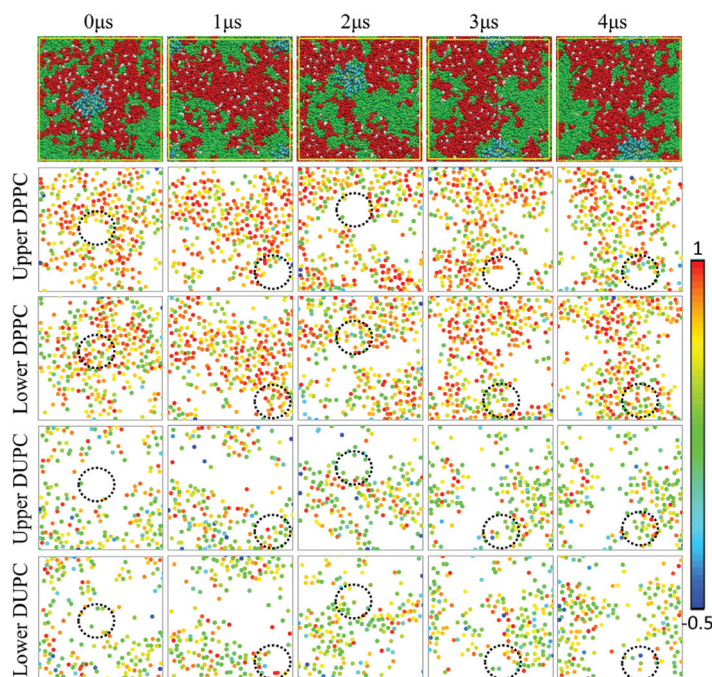

Fig. 5 Time evolution of system snapshots and lipid order parameters for C1–P1 Janus NP-embedded lipid membrane systems. For the snapshot, the coloring style is the same as in Fig. 1. For the lipid chain order map, each point represents one DPPC/DUPC molecule, and its color shows the averaged chain order parameters. The dashed black circle indicates the localization of the C1–P1 Janus NP.

ligand amphiphilicity can affect both the two above-mentioned processes and thus determines the final raft affinity.

Amphiphilic Janus NP show negligible effects on the overall properties of phase-separated lipid membranes

In order to evaluate the effect of membrane-bound Janus NPs on the general properties of phase-separated lipid bilayers, we focused on important indicators of lipid raft dynamics.[5,56] Hence, we obtained the normalized lateral contact of unsaturated lipids (Fig. S3†), the lipid chain order parameters (Fig. S4a†) and cholesterol preference (Fig. S4b†). The results clearly showed that the membrane-bound Janus NP has no significant effects on the overall properties of phase-separated lipid membranes, which is consistent with the work of Yang *et al.*[51] Besides, a 2D phase map was used to show the location of each lipid and its corresponding chain order parameters. For Janus NPs targeting the lipid raft (C1–P1, Fig. 5; C1–P5, Fig. S6†), the chain order parameters of the surrounding lipids become slightly smaller (disorder) than other saturated lipids far away from the Janus NP. This is probably because the insertion of the Janus NP may induce local membrane bending, which further causes disruption to the surrounding tightly packed lipids.[57,58] Differently, chains of unsaturated lipids are much more flexible and disordered, and can easily adapt to the insertion of Janus NPs. Hence, Janus NPs targeting the lipid non-raft (C5–P1, Fig. S7; C5–P5, Fig. S8†) did not induce obvious local disturbance to the lipid chain order. Besides, in all cases, Janus NPs have little effects to the membrane leaflet opposite to the membrane leaflet they inserted into.

In order to further explore the local disturbance of Janus NPs to the lipid membrane region, we then quantified the local membrane packing and thickness. As shown in Fig. 6a, the area of the corresponding lipid was represented by each Voronoi polygon, which was colored according to its value. For Janus NPs with either high or low raft affinity, the area per

lipid of the region where Janus NPs were inserted was significantly increased. In particular, the situation of less hydrophobic Janus NPs (C5–P1 and C5–P5) was much more obvious than that of more hydrophobic Janus NPs (C1–P1 and C1–P5). The reason is that the non-raft domain is loosely packed and has a larger area per lipid, which can be more easily disrupted by these Janus NPs. However, in all cases, membrane-bound Janus NPs did not significantly change the overall thickness of the phase-separated lipid membrane (Fig. 6b). It is worth mentioning that there is no significant disruption to the lipid membrane by our Janus NPs in our MD simulations, which is different from that for the Janus NP of 100 nm or so reported in experiments.[6,30,59] This is probably due to the differences in the size and concentration of Janus NPs, which should be con-
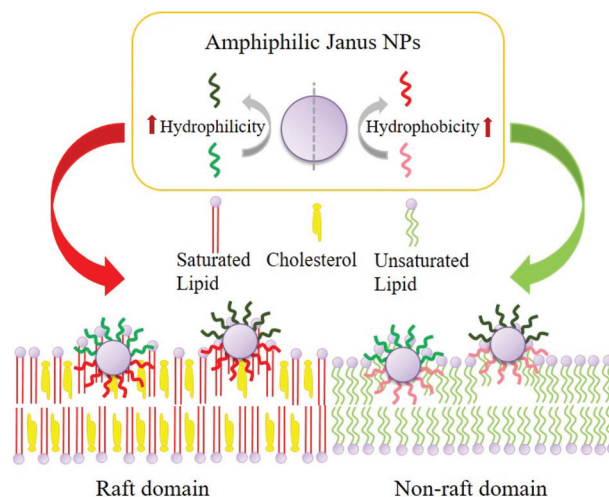
Scheme 1 The preferred localization of Janus nanoparticles can be tuned by adjusting their surface ligand hydrophobicity and their membrane insertion depth can be modulated by the surface ligand hydrophilicity.
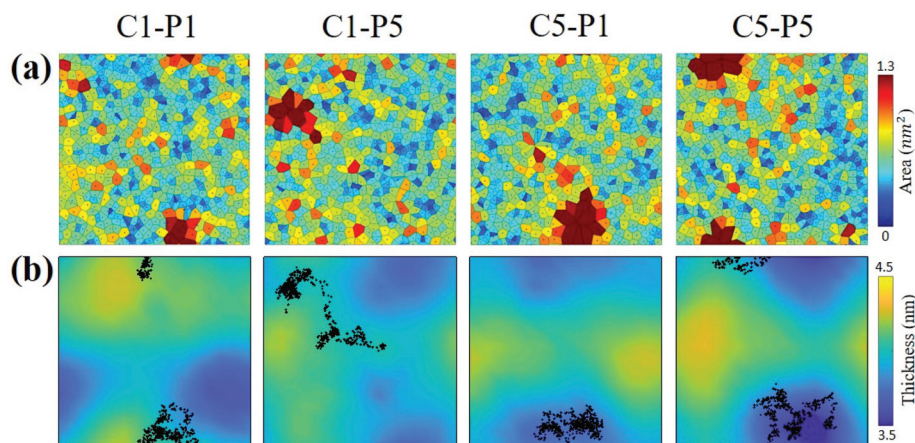

Fig. 6 Effects of membrane-bound Janus NPs on local area per lipid and thickness of the membrane. (a) 2D Voronoi tessellation analysis of lipids in the upper membrane leaflet in the $x−y$ plane at the end of 4 μs trajectory. The dots denote the COM of the DPPC/DUPC/CHOL molecules. Area per lipid is represented by the polygon area, which is colored according to its value. (b) Local membrane thickness for simulation systems averaged over the last 500 ns. The black point corresponds to the NP's trajectory projected in the $x−y$ plane.

sidered in the final applications of these Janus NPs for targeting and regulating lipid rafts.

Conclusions

In this work, we focused on the roles of the surface ligand amphiphilicity in membrane partitioning and targeting thermodynamics of amphiphilic Janus NPs using a series of µs-scale CGMD simulations and umbrella sampling free energy calculations. Through different ligand hydrophobicity (C1, C5; C1 > C5) and ligand hydrophilicity (P1, P5; P1 < P5), we found that the lateral membrane partitioning thermodynamics of Janus NP was mainly determined by their surface ligand hydrophobicity (Scheme 1), while its membrane targeting ability to either lipid raft or non-raft domains is jointly modulated by ligand hydrophobicity and hydrophilicity. Both the membrane targeting and lateral membrane partitioning processes contribute to the final lipid raft affinity of Janus NPs. In our simulations, the C1–P5 Janus NP inserted into the lipid membrane shows the highest lateral partitioning ability to lipid raft, while C1–P1 exhibits the best targeting ability to the lipid raft from the bulk water region. Compared to C5–P5, C5–P1 has better targeting ability and consistent lateral partitioning ability to lipid non-raft. Besides, the ultra-small Janus NPs in this work show no significant disruption to the overall properties of the phase-separated lipid membrane except for the local disturbance. These results may provide useful insights into the design of functional Janus NPs with tunable raft affinity for targeting and regulating lipid rafts.

Author contributions

Conceptualization: X. B. L.; methodology: X. B. L., X. Q. L.; formal analysis: X. Q. L., X. B. L.; investigation and visualization: X. Q. L., X. B. L.; writing-original draft: X. Q. L.; writing-review and editing: X. B. L.; funding acquisition: X. B. L.; project administration: X. B. L. All authors have read and agreed to the published version of the manuscript.

Conflicts of interest

The authors declare no competing interests.

Acknowledgements

References

1 E. Sezgin, I. Levental, S. Mayor and C. Eggeling, The Mystery of Membrane Organization: Composition, Regulation and Roles of Lipid Rafts, *Nat. Rev. Mol. Cell Biol.*, 2017, **18**, 361–374.

2 I. Levental, K. R. Levental and F. A. Heberle, Lipid Rafts: Controversies Resolved, Mysteries Remain, *Trends Cell Biol.*, 2020, **30**, 341–353.

3 D. Lingwood and K. Simons, Lipid Rafts as a Membrane-Organizing Principle, *Science*, 2010, **327**, 46–50.

4 A. Ghysels, A. Kramer, R. M. Venable, W. E. Teague Jr., E. Lyman, K. Gawrisch and R. W. Pastor, Permeability of Membranes in the Liquid Ordered and Liquid Disordered Phases, *Nat. Commun.*, 2019, **10**, 5616.

5 X. Lin, J. H. Lorent, A. D. Skinkle, K. R. Levental, M. N. Waxham, A. A. Gorfe and I. Levental, Domain Stability in Biomimetic Membranes Driven by Lipid Polyunsaturation, *J. Phys. Chem. B*, 2016, **120**, 11930–11941.

6 K. Lee and Y. Yu, Lipid Bilayer Disruption Induced by Amphiphilic Janus Nanoparticles: The Non-Monotonic Effect of Charged Lipids, *Soft Matter*, 2019, **15**, 2373–2380.

7 X. Lin, Z. Li and A. A. Gorfe, Reversible Effects of Peptide Concentration and Lipid Composition on H-Ras Lipid Anchor Clustering, *Biophys. J.*, 2015, **109**, 2467–2470.

8 J. D. Nickels, J. C. Smith and X. Cheng, Lateral Organization, Bilayer Asymmetry, and Inter-Leaflet Coupling of Biological Membranes, *Chem. Phys. Lipids*, 2015, **192**, 87–99.

9 X. Lin, S. Zhang, H. Ding, I. Levental and A. A. Gorfe, The Aliphatic Chain of Cholesterol Modulates Bilayer Interleaflet Coupling and Domain Registration, *FEBS Lett.*, 2016, **590**, 3368–3374.

10 S. Zhang and X. Lin, Lipid Acyl Chain Cis Double Bond Position Modulates Membrane Domain Registration/Anti-Registration, *J. Am. Chem. Soc.*, 2019, **141**, 15884–15890.

11 A. El-Sayed and H. Harashima, Endocytosis of Gene Delivery Vectors: From Clathrin-Dependent to Lipid Raft-Mediated Endocytosis, *Mol. Ther.*, 2013, **21**, 1118–1130.

12 P. Panja and N. R. Jana, Lipid-Raft-Mediated Direct Cytosolic Delivery of Polymer-Coated Soft Nanoparticles, *J. Phys. Chem. B*, 2020, **124**, 5323–5333.

13 M. A. Alonso and J. Millán, The Role of Lipid Rafts in Signalling and Membrane Trafficking in T Lymphocytes, *J. Cell Sci.*, 2001, **114**, 3957–3965.

14 T. Taguchi and K. Mukai, Innate Immunity Signalling and Membrane Trafficking, *Curr. Opin. Cell Biol.*, 2019, **59**, 1–7.

15 P. Varshney, V. Yadav and N. Saini, Lipid Rafts in Immune Signalling: Current Progress and Future Perspective, *Immunology*, 2016, **149**, 13–24.

16 S. Y. Lee, S.-H. Ko, J.-S. Shim, D.-D. Kim and H.-J. Cho, Tumor Targeting and Lipid Rafts Disrupting Hyaluronic Acid-Cyclodextrin-Based Nanoassembled Structure for Cancer Therapy, *ACS Appl. Mater. Interfaces*, 2018, **10**, 36628–36640.

17 V. O. Shipunova, E. N. Komedchikova, P. A. Kotelnikova, I. V. Zelepukin, A. A. Schulga, G. M. Proshkina,

E. I. Shramova, H. L. Kutscher, G. B. Telegin and A. V. Kabashin, Dual Regioselective Targeting the Same Receptor in Nanoparticle-Mediated Combination Immuno/Chemotherapy for Enhanced Image-Guided Cancer Treatment, *ACS Nano*, 2020, **14**, 12781–12795.

18 S. Sensale, Z. Ramshani, S. Senapati and H.-C. Chang, Universal Features of Non-Equilibrium Ionic Currents through Perm-Selective Membranes: Gating by Charged Nanoparticles/Macromolecules for Robust Biosensing Applications, *J. Phys. Chem. B*, 2021, **125**, 1906–1915.

19 M. Ramezanpour, S. Leung, K. Delgado-Magnero, B. Bashe, J. Thewalt and D. Tieleman, Computational and Experimental Approaches for Investigating Nanoparticle-Based Drug Delivery Systems, *Biochim. Biophys. Acta, Biomembr.*, 2016, **1858**, 1688–1709.

20 G. Chen, I. Roy, C. Yang and P. N. Prasad, Nanochemistry and Nanomedicine for Nanoparticle-Based Diagnostics and Therapy, *Chem. Rev.*, 2016, **116**, 2826–2885.

21 X. Bai, S. Wang, X. Yan, H. Zhou, J. Zhan, S. Liu, V. K. Sharma, G. Jiang, H. Zhu and B. Yan, Regulation of Cell Uptake and Cytotoxicity by Nanoparticle Core under the Controlled Shape, Size, and Surface Chemistries, *ACS Nano*, 2019, **14**, 289–302.

22 X. Lin, X. Lin and N. Gu, Optimization of Hydrophobic Nanoparticles to Better Target Lipid Rafts with Molecular Dynamics Simulations, *Nanoscale*, 2020, **12**, 4101–4109.

23 X. Lin and X. Lin, Surface Ligand Rigidity Modulates Lipid Raft Affinity of Ultra-Small Hydrophobic Nanoparticles: Insights from Molecular Dynamics Simulations, *Nanoscale*, 2021, **13**, 9825–9833.

24 P. Choo, T. Liu and T. W. Odom, Nanoparticle Shape Determines Dynamics of Targeting Nanoconstructs on Cell Membranes, *J. Am. Chem. Soc.*, 2021, **143**, 4550–4555.

25 K.-S. Kim, J.-H. Han, S. H. Choi, H.-Y. Jung, J. D. Park, H.-J. An, S.-E. Kim, D.-H. Kim, J. Doh and D. K. Han, Cationic Nanoparticle-Mediated Activation of Natural Killer Cells for Effective Cancer Immunotherapy, *ACS Appl. Mater. Interfaces*, 2020, **12**, 56731–56740.

26 G. Agrawal and R. Agrawal, Janus Nanoparticles: Recent Advances in Their Interfacial and Biomedical Applications, *ACS Appl. Nano Mater.*, 2019, **2**, 1738–1757.

27 J. Fu, D. An, Y. Song, C. Wang, M. Qiu and H. Zhang, Janus Nanoparticles for Cellular Delivery Chemotherapy: Recent Advances and Challenges, *Coord. Chem. Rev.*, 2020, **422**, 213467.

28 L. Zhang, M. Zhang, L. Zhou, Q. Han, X. Chen, S. Li, L. Li, Z. Su and C. Wang, Dual Drug Delivery and Sequential Release by Amphiphilic Janus Nanoparticles for Liver Cancer Theranostics, *Biomaterials*, 2018, **181**, 113–125.

29 K. Lee and Y. Yu, Lipid Bilayer Disruption by Amphiphilic Janus Nanoparticles: The Role of Janus Balance, *Langmuir*, 2018, **34**, 12387–12393.

30 K. Lee, L. Zhang, Y. Yi, X. Wang and Y. Yu, Rupture of Lipid Membranes Induced by Amphiphilic Janus Nanoparticles, *ACS Nano*, 2018, **12**, 3646–3657.

31 L. Ou, V. Corradi, D. P. Tieleman and Q. Liang, Atomistic Simulations on Interactions between Amphiphilic Janus Nanoparticles and Lipid Bilayers: Effects of Lipid Ordering and Leaflet Asymmetry, *J. Phys. Chem. B*, 2020, **124**, 4466–4475.

32 X. Li, L. Zhou, Y. Wei, A. M. El-Toni, F. Zhang and D. Zhao, Anisotropic Growth-Induced Synthesis of Dual-Compartment Janus Mesoporous Silica Nanoparticles for Bimodal Triggered Drugs Delivery, *J. Am. Chem. Soc.*, 2014, **136**, 15086–15092.

33 P. W. Fowler, J. J. Williamson, M. S. P. Sansom and P. D. Olmsted, Roles of Interleaflet Coupling and Hydrophobic Mismatch in Lipid Membrane Phase-Separation Kinetics, *J. Am. Chem. Soc.*, 2016, **138**, 11633–11642.

34 D. R. Elias, A. Poloukhtine, V. Popik and A. Tsourkas, Effect of Ligand Density, Receptor Density, and Nanoparticle Size on Cell Targeting, *Nanomedicine*, 2013, **9**, 194–201.

35 S. J. Marrink, H. J. Risselada, S. Yefimov, D. P. Tieleman and A. H. De Vries, The Martini Force Field: Coarse Grained Model for Biomolecular Simulations, *J. Phys. Chem. B*, 2007, **111**, 7812–7824.

36 S. J. Marrink, V. Corradi, P. C. T. Souza, H. I. Ingólfsson, D. P. Tieleman and M. S. P. Sansom, Computational Modeling of Realistic Cell Membranes, *Chem. Rev.*, 2019, **119**, 6184–6226.

37 R. Alessandri, F. Grünewald and S. J. Marrink, The Martini Model in Materials Science, *Adv. Mater.*, 2021, **33**, 2008635.

38 J. Lin, H. Zhang, Z. Chen and Y. Zheng, Penetration of Lipid Membranes by Gold Nanoparticles: Insights into Cellular Uptake, Cytotoxicity, and Their Relationship, *ACS Nano*, 2010, **4**, 5421–5429.

39 N. B. Shah, G. M. Vercellotti, J. G. White, A. Fegan, C. R. Wagner and J. C. Bischof, Blood–Nanoparticle Interactions and in Vivo Biodistribution: Impact of Surface Peg and Ligand Properties, *Mol. Pharm.*, 2012, **9**, 2146–2155.

40 M. Bloemen, T. Van Stappen, P. Willot, J. Lammertyn, G. Koeckelberghs, N. Geukens, A. Gils and T. Verbiest, Heterobifunctional Peg Ligands for Bioconjugation Reactions on Iron Oxide Nanoparticles, *PLoS One*, 2014, **9**, e109475.

41 Y. Zhong, F. Peng, X. Wei, Y. Zhou, J. Wang, X. Jiang, Y. Su, S. Su, S. T. Lee and Y. He, Microwave–Assisted Synthesis of Biofunctional and Fluorescent Silicon Nanoparticles Using Proteins as Hydrophilic Ligands, *Angew. Chem.*, 2012, **124**, 8613–8617.

42 Z. Zeng, Y. Hoshino, A. Rodriguez, H. Yoo and K. J. Shea, Synthetic Polymer Nanoparticles with Antibody-Like Affinity for a Hydrophilic Peptide, *ACS Nano*, 2010, **4**, 199–204.

43 T. A. Wassenaar, H. I. Ingólfsson, R. A. Böckmann, D. P. Tieleman and S. J. Marrink, Computational Lipidomics with Insane: A Versatile Tool for Generating Custom Membranes for Molecular Simulations, *J. Chem. Theory Comput.*, 2015, **11**, 2144–2155.

44 S. Pronk, S. Páll, R. Schulz, P. Larsson, P. Bjelkmar, R. Apostolov, M. R. Shirts, J. C. Smith, P. M. Kasson and D. van der Spoel, Gromacs 4.5: A High-Throughput and Highly Parallel Open Source Molecular Simulation Toolkit, *Bioinformatics*, 2013, **29**, 845–854.

45 M. Parrinello and A. Rahman, Polymorphic Transitions in Single Crystals: A New Molecular Dynamics Method, *J. Appl. Phys.*, 1981, **52**, 7182–7190.

46 G. Bussi, D. Donadio and M. Parrinello, Canonical Sampling through Velocity Rescaling, *J. Chem. Phys.*, 2007, **126**, 014101.

47 W. Humphrey, A. Dalke and K. Schulten, Vmd: Visual Molecular Dynamics, *J. Mol. Graphics*, 1996, **14**, 33–38.

48 S. Kumar, J. M. Rosenberg, D. Bouzida, R. H. Swendsen and P. A. Kollman, The Weighted Histogram Analysis Method for Free–Energy Calculations on Biomolecules. I. The Method, *J. Comput. Chem.*, 1992, **13**, 1011–1021.

49 W. D. Bennett and D. P. Tieleman, Computer Simulations of Lipid Membrane Domains, *Biochim. Biophys. Acta, Bioenerg.*, 2013, **1828**, 1765–1776.

50 X. Lin and A. A. Gorfe, Understanding Membrane Domain-Partitioning Thermodynamics of Transmembrane Domains with Potential of Mean Force Calculations, *J. Phys. Chem. B*, 2019, **123**, 1009–1016.

51 K. Yang, R. Yang, X. Tian, K. He, S. L. Filbrun, N. Fang, Y. Ma and B. Yuan, Partitioning of Nanoscale Particles on a Heterogeneous Multicomponent Lipid Bilayer, *Phys. Chem. Chem. Phys.*, 2018, **20**, 28241–28248.

52 Q. J. Ji, B. Yuan, X. M. Lu, K. Yang and Y. Q. Ma, Controlling the Nanoscale Rotational Behaviors of Nanoparticles on the Cell Membranes: A Computational Model, *Small*, 2016, **12**, 1140–1146.

53 Z. Li, L. Janosi and A. A. Gorfe, Formation and Domain Partitioning of H-Ras Peptide Nanoclusters: Effects of Peptide Concentration and Lipid Composition, *J. Am. Chem. Soc.*, 2012, **134**, 17278–17285.

54 L. Janosi, Z. Li, J. F. Hancock and A. A. Gorfe, Organization, Dynamics, and Segregation of Ras Nanoclusters in Membrane Domains, *Proc. Natl. Acad. Sci. U. S. A.*, 2012, **109**, 8097–8102.

55 X. Lin, A. A. Gorfe and I. Levental, Protein Partitioning into Ordered Membrane Domains: Insights from Simulations, *Biophys. J.*, 2018, **114**, 1936–1944.

56 D. Marguet, P. F. Lenne, H. Rigneault and H. T. He, Dynamics in the Plasma Membrane: How to Combine Fluidity and Order, *EMBO J.*, 2006, **25**, 3446–3457.

57 K. He, Y. Wei, Z. Zhang, H. Chen, B. Yuan, H.-B. Pang and K. Yang, Membrane-Curvature-Mediated Co-Endocytosis of Bystander and Functional Nanoparticles, *Nanoscale*, 2021, **13**, 9626–9633.

58 S. Sonnino and A. Prinetti, Membrane Domains and the "Lipid Raft" Concept, *Curr. Med. Chem.*, 2013, **20**, 4–21.

59 J. T. Wiemann, Z. Shen, H. Ye, Y. Li and Y. Yu, Membrane Poration, Wrinkling, and Compression: Deformations of Lipid Vesicles Induced by Amphiphilic Janus Nanoparticles, *Nanoscale*, 2020, **12**, 20326–20336.